Contents I

Chapter 1: Introduction

Cymbidium mosaic potexvirus (CymMV) and odontoglossum ringspot tobamovirus (ORSV) are the most prevalent and economically important viruses [1-4]. CymMV induces floral and foliar necrosis (Figure 1). ORSV causes ring spots on leaves and color breaking on flowers. Co-infections of both viruses cause blossom brown necrotic streak. The virus reduces plant vigor and flower quality, thus influencing the economic value [5].

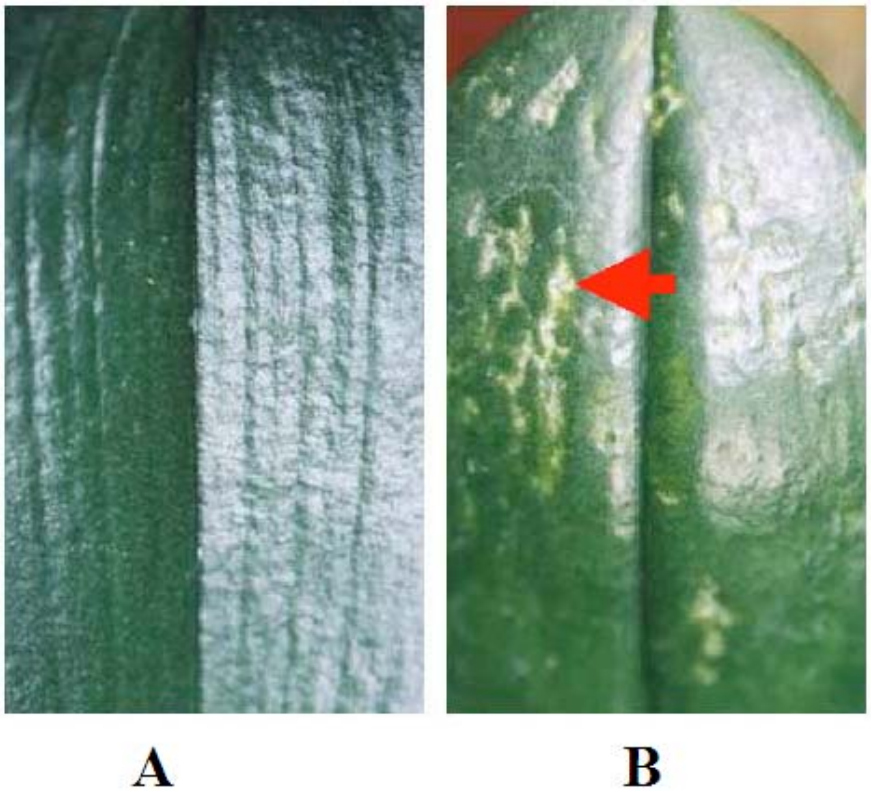

Figure 1. CymMV induce the mosaic of orchid leaf. (A) healthy (B) CymMV infected, the red arrow indicated the mosaic of the leaf.

A number of methods have been developed to analyze CymMV, e.g., enzyme-linked immunosorbent assay (ELISA) [6, 7], liquid chromatography-mass spectrometry (LC-MS) and matrix-assisted laser desorption-ionization (MALDI) [8], reverse transcription polymerase chain reaction (RT–PCR) [9], immuno-capillary zone electrophoresis (I-CZE) [10], and DIG-labeled cRNA probes [11]. Some of these methods require additional time-consuming labeling and amplification procedures. These methods are sensitive; however, they require hours and trained personnel to obtain unambiguous results.

A QCM is a mass detection device (Figure 2) that operates based on the piezoelectric properties of quartz crystal [12-14]. QCMs are unsophisticated and cost-effective, have a real-time response and a high resolution, and are stable. Therefore, QCMs have been applied in recent years as biosensors for the real-time detection of liquid phase samples, such as protein, DNA, RNA, and heavy metal ion solutions. [15-19]. QCMs have also been applied in the detection of CymMV, and provide the advantages of convenience and economy [20]. However, sensitivity and stability might be improved by further modification.

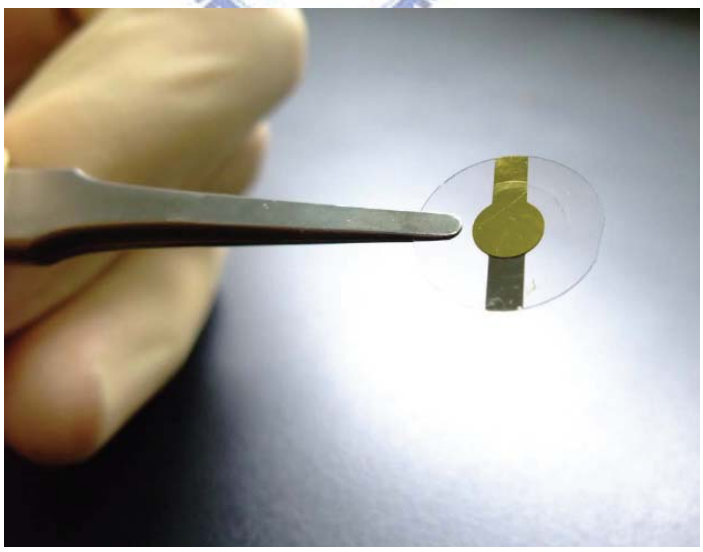

Figure 2. 10MHz QCM

Fabrication of nanostructures on the interfaces of biosensors often leads to vast improvements, including significantly enhanced sensitivities with deposition of nanoparticles onto optical sensors [21] and surface plasmon resonance sensors [22], nanowire- [23] and

nanotube- [24] functionalization of FET sensors, and the use of other nano-scale sensors [25]. Surface modification of QCM electrodes is also performed using single-wall carbon nanotubes (SWNT) [26]. However, enhancements in sensitivity and stability and application to field detection have yet to be demonstrated.

The current study is based on SWNT-modified QCM sensors and applies to the detection of CymMV. Compared to traditional detection methods, our study provides a rapid, convenient, and economical method with a comparable sensitivity for quantification of the amount of CymMV in general orchid plants.

Chapter 2: Experiment detail

2.1 QCM experiment

An oscillator (Catalog #35366-10) and a flow cell (Catalog#35363) were purchased from International Crystal Manufacturing Co. (Oklahoma City, USA). The QCM was fabricated from a 0.2-mm thick AT-cut quartz wafer. A laboratory-constructed transistor–transistor logic integrated circuit (TTLIC) was used to power the QCM. An Agilent HP 53132 universal frequency counter was used to monitor the frequency output.

2.2 Fabrication of SWNT-functionalized QCM

A gold electrode was cleaned by immersing in 1.2 M NaOH for 20 min, 1.2 M HCl for 5 min, and distilled water for 5 min. After a final rinse with 95% ethanol, it was air-dried at room temperature.

A typical SWNT film was formed on a quartz crystal surface by first dispersing bulk SWNTs (Sigma) produced by high-pressure CO in chloroform at a concentration of 50 μg mL^{-1}. One hundred microliters of this suspension was then deposited onto the crystal surface dropwise and baked at 60°C for 1 h. Control experiments were done on bare QCM substrates without deposited nanotubes. The sample was examined with atomic force microscopy (AFM) for size and homogeneity.

2.3 Activation of CDI-Tween 20 for Conjugation to anti-CymMV

Five milligrams of Tween 20 (J.T.Baker) and 4.0 g 1,1-carbonyldiimidazole (CDI) (Fluka) were allowed to react in 25 mL DMSO (Fluka; dried under a molecular sieve) at 40°C for 2 h with stirring. Ethyl ether (J.T.Baker) was then added to cause precipitation, after which the precipitates were collected, dissolved in DMSO, and precipitated in ether. This process was repeated twice to ensure the removal of excess CDI, and was followed by drying the intermediate in vacuo overnight [26]. The CDI-Tween 20 composite was examined by FTIR spectrum 100. For conjugation to anti-CymMV antibodies, nanotube samples were first exposed to CDI-Tween 20 (1% w/v in water) for 30 min, and then rinsed thoroughly with water to remove excess reagents. The samples were then incubated in 1 μg mL^{-1} anti-CymMV in PBS buffer for 24 h and washed with PBS buffer for 1 min, then with deionized water. Raman spectroscopy was used to examine each step of modification. Additionally, the frequencies of all QCMs were monitored until steady state conditions were achieved (usually 30 min to 1 h), following which 20 μL of sample was injected.

2.4 ELISA

Each microwell of a 96-well Corning plate was pretreated with 100 μL 3% glutaraldehyde for 30 min at room temperature, followed by phosphate buffered saline (PBS) washing. One hundred microliters of properly diluted CymMV were added to the microwells and incubated for 2 h at room temperature, followed by Milli-Q water washing three times,

and then washing with PBS three times. Blocking for nonspecific binding was performed by adding 100 μL of 3% BSA and incubating for 4 h at room temperature, followed by PBS washing three times.

Binding was performed by adding 100 μL properly diluted antiserum into the microwells and incubating for 1 h at room temperature, followed by thorough washes. Horseradish peroxidase (HRP)-conjugated anti-rabbit IgG, 2,2-azino-bis (3-ethylbenzthiazoline-6-sulfonic acid) (ABTS), and H_2O_2 were added in sequence to the wells according to the manufacturer's protocol, and the binding efficiency was monitored by absorbance at 405 nm.

2.5 CymMV purification and antisera production

CymMV was purified according to Wong and coworkers [27]. Fresh CymMV-infected leaves (100 g) were homogenized in a Waring blender (Waring Products, New Hartford, CT) for 5 min with 500 mL of extraction buffer (0.1% beta-mercaptoethanol, 0.01 M EDTA, and 0.1 M sodium phosphate buffer, pH 7.5). The extract was clarified with 100 mL of chloroform and centrifuged at 8,000 g for 10 min at 4°C. The supernatant was filtered through cheesecloth before sodium chloride (NaCl) and polyethylene glycol (molecular weight 8,000) were added to final concentrations of 0.25 and 4%, respectively. The mixture was centrifuged at 8,000 g for 20 min at 4°C. The pellet was suspended in 5 mL of suspension buffer (1% Triton X-100 and 0.1 M sodium borate buffer, pH 8.0) and stirred slowly for 12 h at 4°C. The suspension was centrifuged at low speed (8,000 g) to remove debris, and the supernatant was

centrifuged at 90,000 g for 2.5 h at 4°C. The pellet was suspended in 2 mL of 0.01 M sodium borate buffer, pH 7.5, and stored at –20°C. The purified CymMVs were characterized by SEM (Figure 3). The CymMV particle lengths ranged from about 40 nm to 550 nm, with widths of approximately 15 nm. The scale bar is 100 nm. To generate infected plants, purified CymMV was injected into the leaves for 2 weeks. The sap was extracted from the diseased leaves (1 g) for detection.

Purified CymMV (1 mg) was suspended in 1 mL of 0.02 M sodium phosphate buffer, pH 7.0, and emulsified with an equal volume of Freund's incomplete adjuvant (Sigma-Aldrich Corp., St. Louis) by vortexing for 1 min. The resulting emulsion was injected intramuscularly into the hind legs of a New Zealand White rabbit. Booster injections of 1 mg each were administered 14, 21, and 28 days after the first injection. Before each booster injection, 10 mL of blood was drawn from the ear of the rabbit. The antiserum collected was divided into 1-mL aliquots and stored at 4°C.

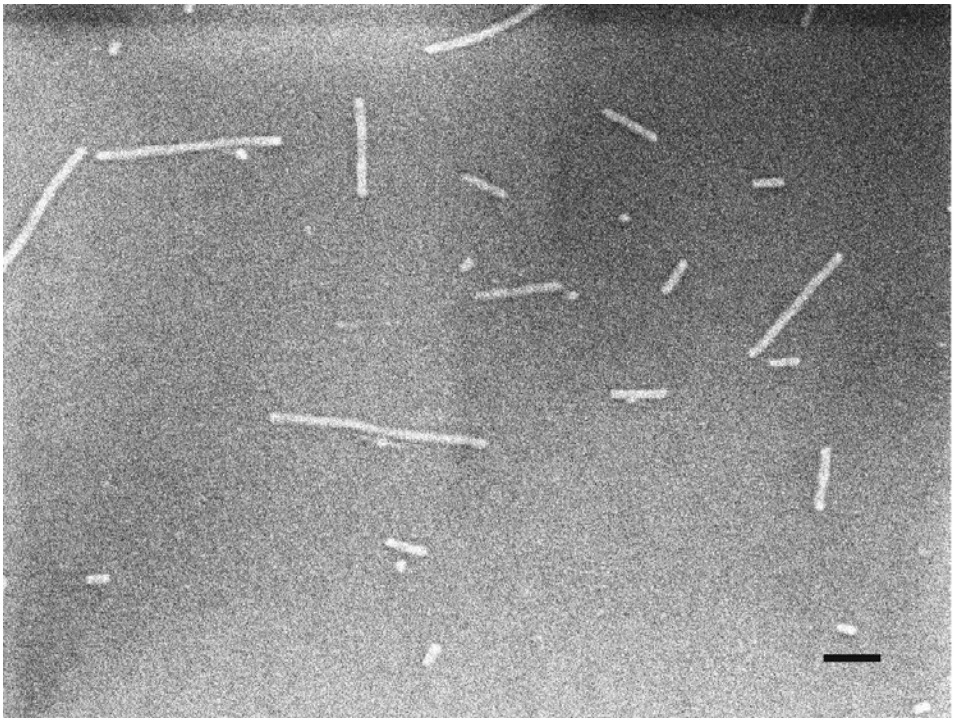

Figure 3. SEM image of purified CymMV. The particle lengths ranged from about 40 nm to 550 nm, with widths of approximately 15 nm. The scale bar is 100 nm.

Chapter 3: Results and discussion

3.1. Fabrication of SWNT-functionalized QCM

Nonspecific binding to SWNTs was found to be a general phenomenon for all proteins examined in recent studies. This spontaneous adsorption onto carbon nanotubes has been attributed to hydrophobic interactions between the proteins and the nanotube surface [28, 29]. In the current study, 1,1'-carbonyldiimidazole-activated Tween 20 (CDI–Tween 20) was conjugated to the side walls of SWNTs by hydrophobic interaction. The antibodies were crosslinked to the amine group of CDI–Tween20 for virus detection (Figure 4).

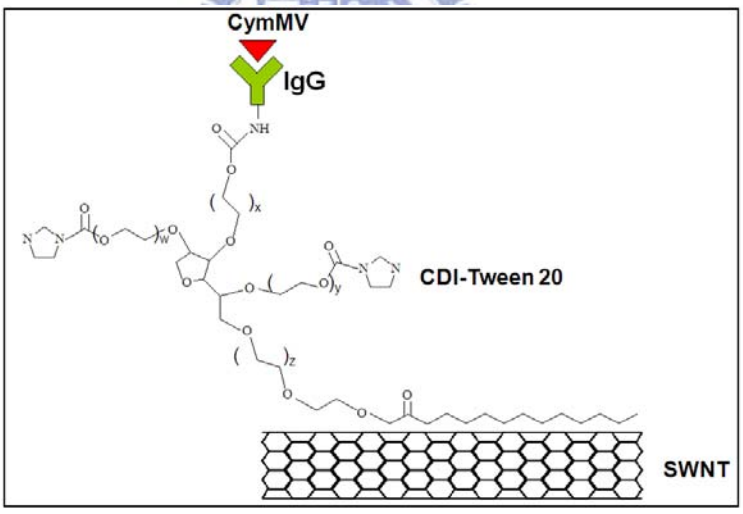

Figure 4. Schematic representation of functionalization with SWNT/CDI-Tween 20 on a QCM. CDI-Tween 20 was conjugated to the side walls of the SWNTs by hydrophobic interaction. The antibodies were crosslinked to the amine group of CDI–Tween20 for virus detection.

High-yield SWNTs were uniformly coated onto the gold electrode of the QCM. The diameter of the SWNTs was 3-5 nm and the length was 1-2 μm, as determined by AFM (Figure 5).

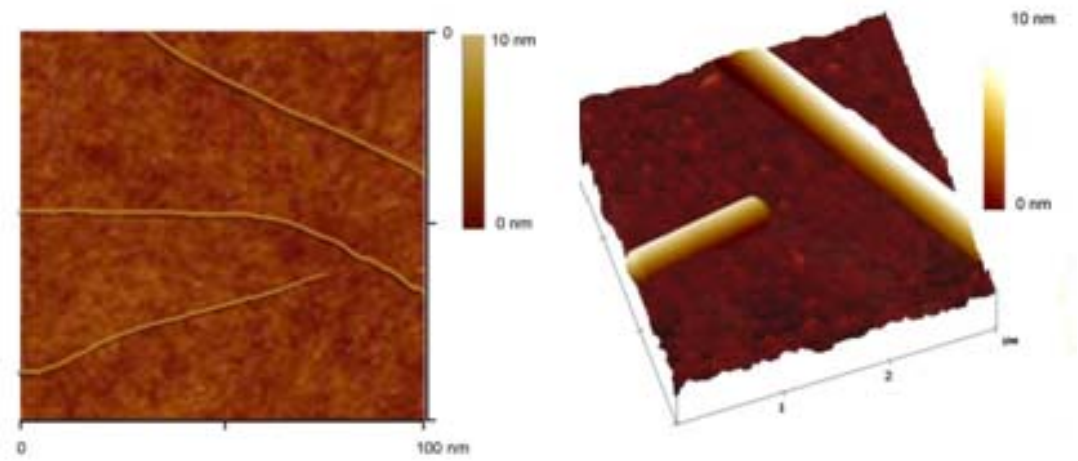

Figure 5. AFM image of the SWNTfunctionalized QCM. The SWNT length is about 1-2 μm and the diameter is 3-5 nm.

The SWNT surface was functionalized with CDI-Tween 20. Tween20 contains functional groups similar to poly(ethylene glycol) (PEG) and a long alkyl chain moiety. PEG moieties were crosslinked to CDI. The synthesis of the CDI–Tween 20 composite was examined by FTIR spectroscopy (Figure 6). The spectrum of Tween 20 is characterized by an O-H stretching band at 3440 cm^{-1}, a C-H band at 2870 cm^{-1}, and a C=O band at 1742 cm^{-1} (Figure 6A). The spectrum of CDI contains a C-H band at 2870 cm^{-1}, a C=O band 1742 cm^{-1}, a C-N band at 1050 cm^{-1}, and a C=N band at 1538 cm^{-1} (Figure 6B). The CDI –Tween 20 conjugate spectrum showed a C-H band at 2924 cm^{-1}, a C-N band at 1744 cm^{-1}, and a C-O

band at 1107 cm^{-1} (Figure 6C). The result demonstrated that the PEG structures were converted to amine groups, as indicated by the disappearance of the O-H peak.

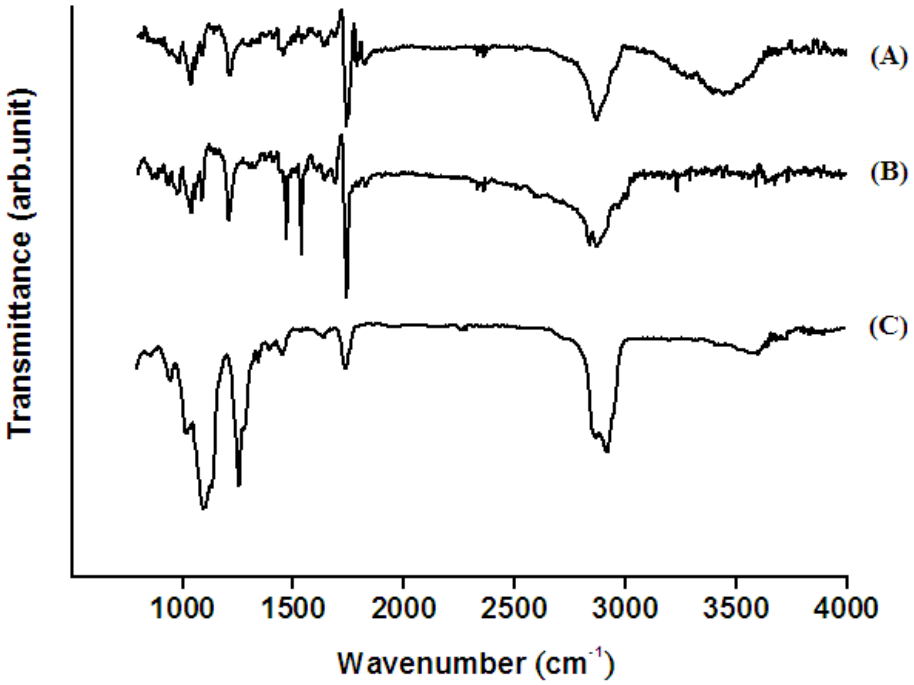

Figure 6. FTIR spectra acquired from the CDI-Tween composite. (A) Tween20, (B) CDI, and (C) CDI-Tween 20.

Raman spectra were used to monitor the step-by-step chemical fabrication (Figure 7). The unique properties of SWNTs arise from their particular one-dimensional structure, which is directly linked to the characteristic Raman bands (G band). The adsorption of SWNTs onto QCMs was characterized by an enhanced G band at 1581 cm^{-1} that dominated the spectra and was significantly stronger than the G' band at 2659 cm^{-1} (Figure 7A).

The functionalization of CDI-Tween 20 to SWNT shifted the G' band to 2664 cm^{-1}, while the G band remained at 1581 cm^{-1} (Figure 7B). The conjugation of the anti-CymMV antibody to CDI-Tween 20/SWNT shifted the G' band to 2675 cm^{-1}, whereas the G band remained at 1581 cm^{-1} (Figure 7C). The frequency shift of the G' band indicated an increase in size of the SWNTs due to the functionalization with CDI-Tween 20 [30].

The functionalization of the SWNTs improved the mechanical and electrical properties. Nonspecific binding of SWNTs was blocked by the conjugated CDI-Tween 20 copolymer chains, thus enhancing the specificity during bio-detection.

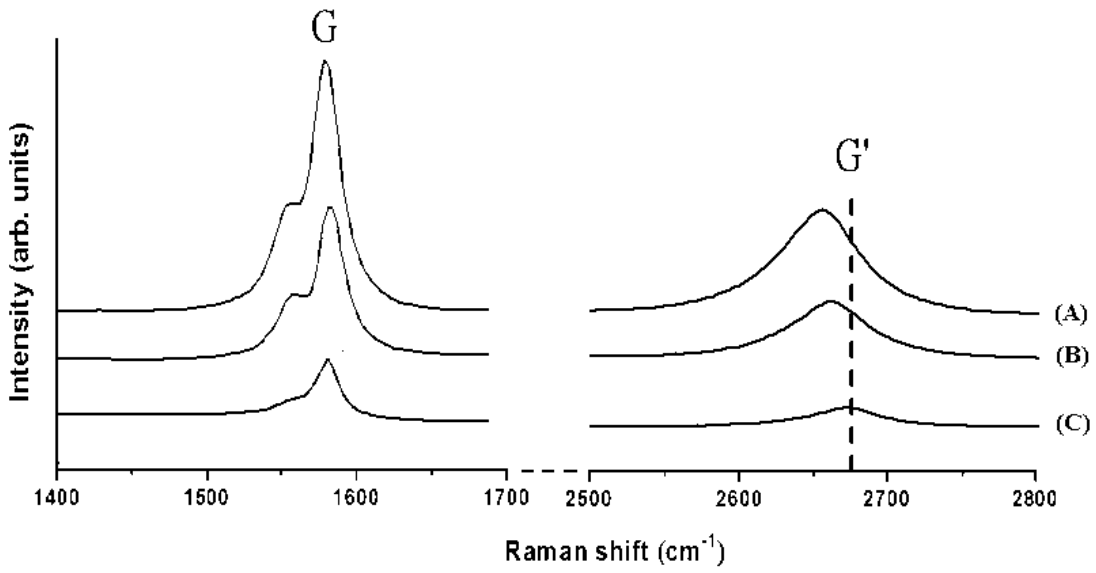

Figure 7. Raman spectra of (A) Purified SWNTs, (B) SWNTs functionalized with CDI-Tween 20, and (C) SWNT/CDI-Tween 20 conjugated to antibodies.

3.2. Detection of CymMV using SWNT-functionalized QCM

The SWNT-functionalized QCM sensors were used for the detection of purified CymMV. The control experiment was performed by immobilizing anti-CymMV antibodies on the naked QCM electrode. Twenty microliters of CymMV at various concentrations were injected into the QCM-FIA system, and the resonant frequency was monitored in real time (Figure 8).

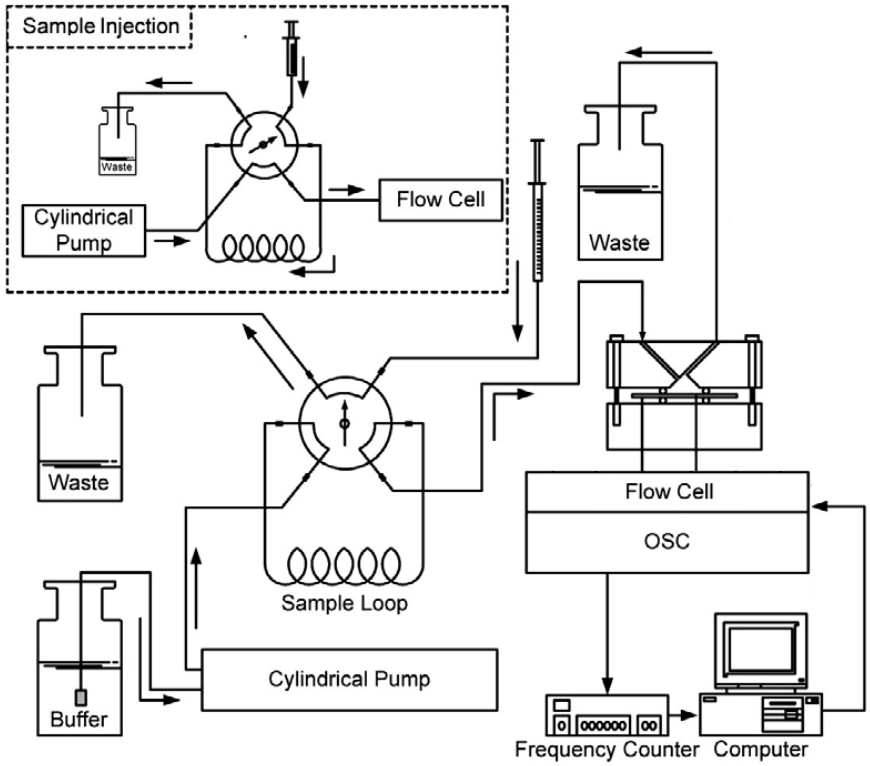

Figure 8. Scheme for the QCM flow injection analysis apparatus. Continuous flow was achieved using a cylindrical pump. The sample was injected through an injection loop and pumped into the flow cell.

Functionalization with CDI-Tween 20 enhanced the frequency response of QCM. The naked electrode responded to 2.08 ng CymMV by 4.5 Hz, while the functionalized QCM respond to 2.08 ng CymMV by 28.91 Hz (figure 9).

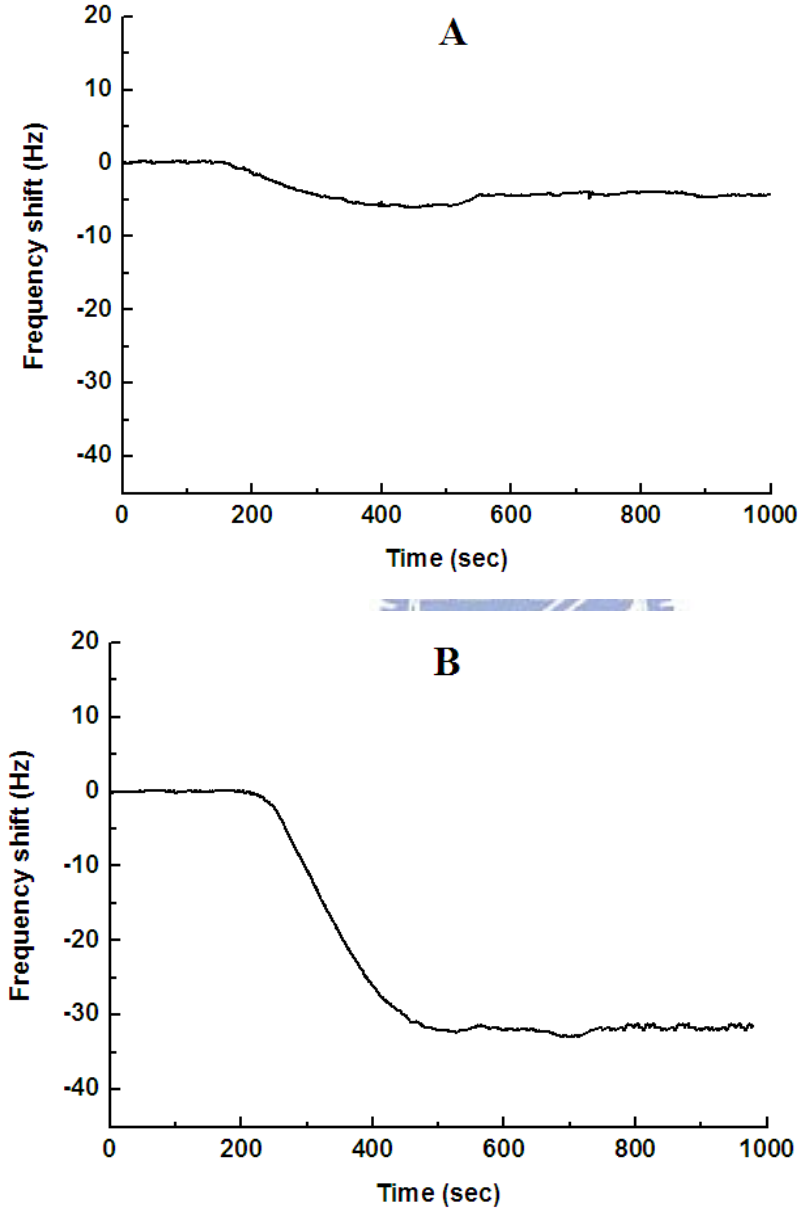

Figure 9. Detection of CymMV using (A) the naked QCM electrode and (B) the SWNT-functionalized QCM. The frequency shift was monitored for injection of 20 μL of CymMV. The concentration of CymMV was 0.1 μg mL^{-1} (2 ng of CymMV).

A 5-fold enhancement in sensitivity was observed at 2.08 ng CymMV, from 2.18 Hz ng^{-1} to 11.56 Hz ng^{-1} (Table 1). The limit of detection (LOD) is defined as three times the standard deviation of the background noise (S/N>3, noise ~0.78 Hz). The LODs of the control experiment and the SWNT functionalization experiment were 2 ng (10^{-4} mg mL^{-1}) and 0.5 ng ($2.5x10^{-5}$ mg mL^{-1}) and the signals were 4.5 Hz and 4.25 Hz, respectively (Figure 10).

Table.1 Comparison of the sensitivities of naked QCMs and SWNT-functionalized QCMs

CymMV (μg mL^{-1})	Sensitivity [a] (Hz ng^{-1})	
	Naked	SWNT/CDI-Tween 20
1.034	3.05	4.55
0.517	4.64	7.13
0.258	2.42	8.08
0.103	2.18	11.5
0.052	2.61	9.89
0.026	1.68	8.22
0.013	3.05	4.54
0.010	4.64	7.13

[a] Sensitivity is defined as the change in frequency shift per applied virus weight. The injection volume is 20 μL. Sensitivity (S) = ΔF/Δm. ΔF: Frequency shift; Δm: applied weight.

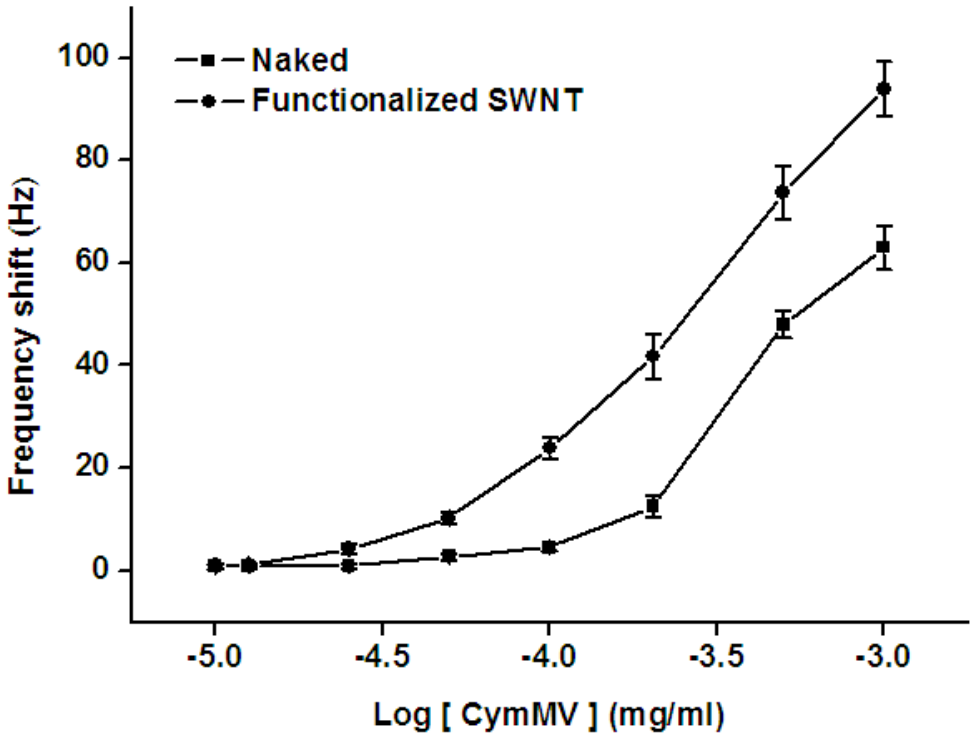

Figure 10. Injection of purified CymMV into the IgG-coated QCM sensor. The QCM electrode was coated with IgG antiserum by naked SWNTs and SWNTs functionalized with CDI-Tween 20. The frequency shift was measured after injection of 20 μL of purified CymMV.

Immuno-detection by ELISA is the most popular method for CymMV detection. The purified CymMV was therefore also examined by ELISA (Figure 11). The LOD of ELISA was 0.13 ng ($1.29x10^{-6}$ mg mL^{-1}, 100 μL per well). The sensitivity and LOD of the functionalized QCM sensors were comparable to ELISA.

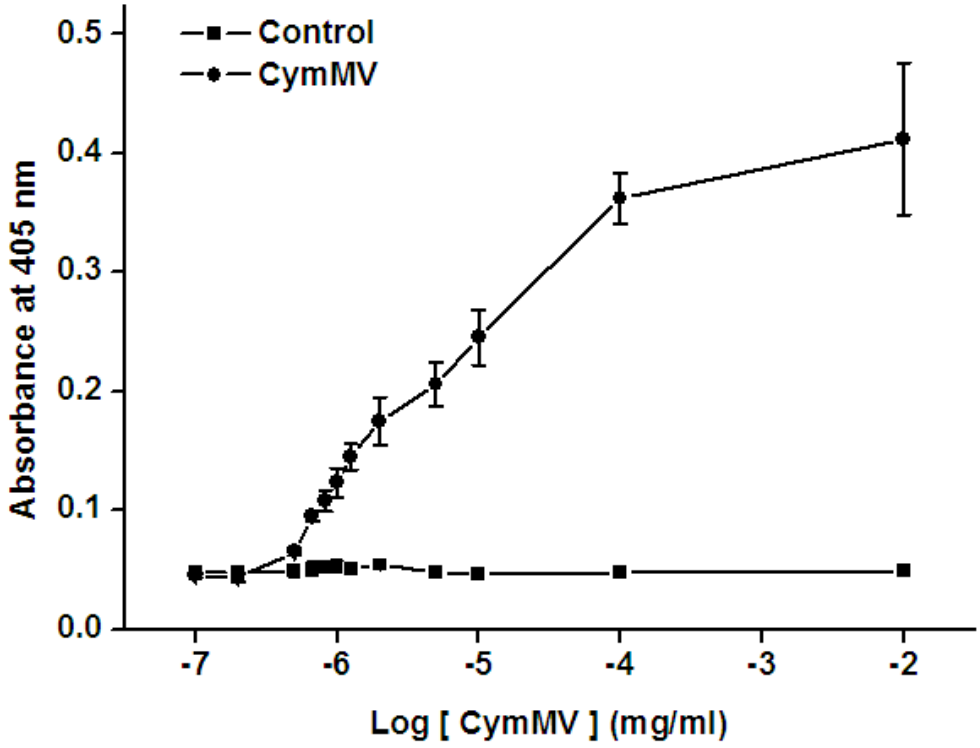

Figure 11. ELISA characterization of purified virus at various concentrations.

Our platform was also successfully used for field detection of CymMV using infected orchid leaves (Figure 12). The detection of CymMV was performed for 11 orchids (including 10 infected plants and 1 healthy plant) using the SWNT-functionalized QCM sensor. The amount of virus per gram of leaves was between 11.5–40.2 μg viruses per gram of leaves (Figure 13). The uninfected orchid showed negative results in the detection.

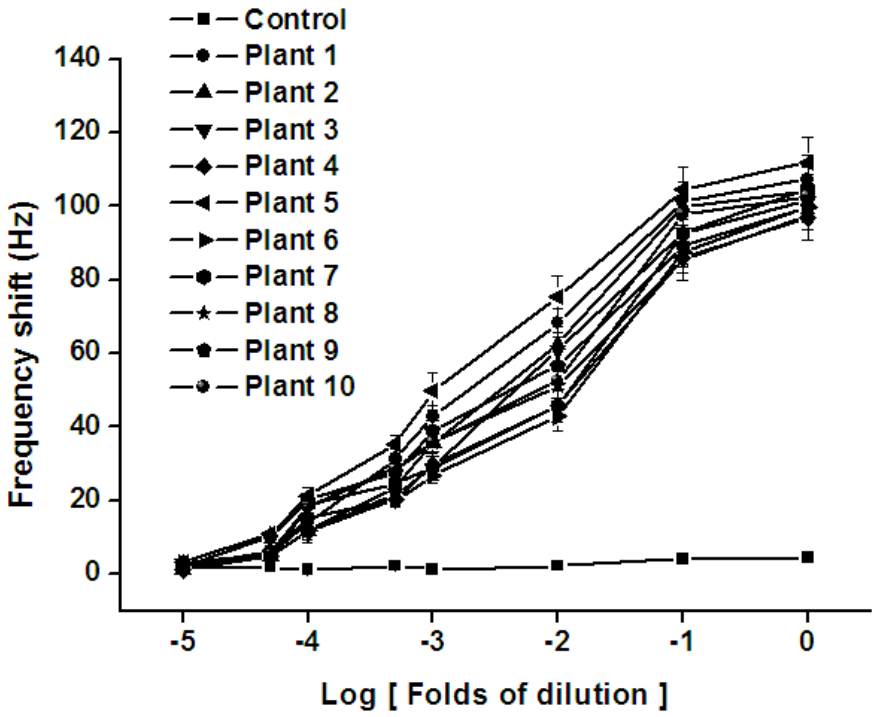

Figure 12. Infected orchid leaf detection using a SWNT-functionalized QCM sensor. The extracted sap samples were from the leaves of 11 plants (including 10 infected plants and 1 healthy plant).

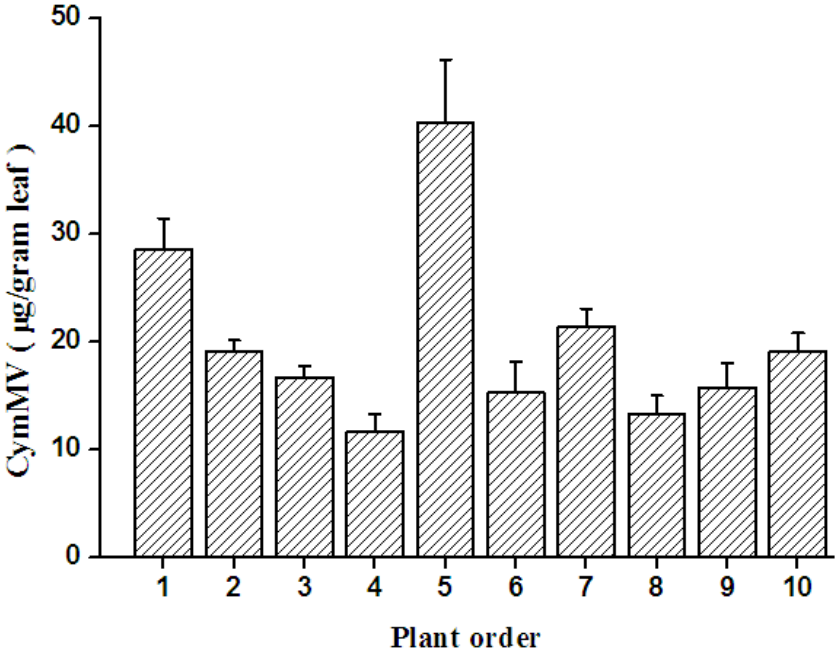

Figure 13. Quantification of the amount of CymMV per gram of leaves. The quantity of CymMV was calculated using a purified CymMV standard curve.

4. Conclusion

We have developed an ultra-sensitive, convenient real-time platform for detecting CymMV based on SWNT-functionalized QCM sensors. Sensitivity was enhanced from 2.18 Hz ng^{-1} to 11.5 Hz ng^{-1} when 0.1 μg mL^{-1} CymMV was applied. The low limit of detection of SWNT-functionalized QCM sensors was improved from 2.08 ng to 0.502 ng. The SWNT-functionalized QCM sensor was successfully used to quantify the amount of CymMV in infected orchid leaves. Compared to ELISA, SWNT-functionalized QCM sensors are fast, economical and ultra-sensitive, with comparable sensitivity. The current study demonstrates that QCMs are a convenient platform for the detection and quantification of CymMV.

References

[1] Zettler F W, Ko N J, Wisler G C, Elliott M S and Wong S M 1990 Viruses of Orchids and Their Control *Plant Disease* **74** 621-6

[2] Ryu K, Park W, Chung S and Yoon K 1995 Occurrence of cymbidium mosaic virus and odontoglossum ringspot virus in Korea *Plant Disease* **79** 321

[3] Liao L, Pan I, Chan Y, Hsu Y, Chen W and Chan M 2004 Transgene silencing in Phalaenopsis expressing the coat protein of Cymbidium Mosaic Virus is a manifestation of RNA-mediated resistance *Molecular Breeding* **13** 229-42

[4] Moles M, Delatte H, Farreyrol K and Grisoni M 2007 Evidence that Cymbidium mosaic virus (CymMV) isolates divide into two subgroups based on nucleotide diversity of coat protein and replicase genes *Archives of Virology* **152** 705-15

[5] Pearson M N and Cole J S 1991 Further Observations on the Effects of Cymbidium Mosaic-Virus and Odontoglossum Ringspot Virus on the Growth of Cymbidium Orchids *Journal of Phytopathology-Phytopathologische Zeitschrift* **131** 193-8

[6] Vejaratpimol R, Channuntapipat C, Liewsaree P, Pewnim T, Ito K, Iizuka M and Minamiura N 1998 Evaluation of enzyme-linked immunosorbent assays for the detection of Cymbidium mosaic virus in orchids *Journal of Fermentation and Bioengineering* **86** 65-71

[7] Grisoni M, Davidson F, Hyrondelle C, Farreyrol K, Caruana M and Pearson M 2004

Nature, incidence, and symptomatology of viruses infecting Vanilla tahitensis in French Polynesia *Plant Disease* **88** 119-24

[8] Tan S W, Wong S M and Kini R M 2000 Rapid simultaneous detection of two orchid viruses using LC- and/or MALDI-mass spectrometry *J Virol Methods* **85** 93-9

[9] Eun A J C, Seoh M L and Wong S M 2000 Simultaneous quantitation of two orchid viruses by the TaqMan (R) real-time RT-PCR *Journal of Virological Methods* **87** 151-60

[10] Eun A and Wong S 1999 Detection of Cymbidium mosaic potexvirus and Odontoglossum ringspot tobamovirus using immuno-capillary zone electrophoresis *Phytopathology* **89** 522-8

[11] Hu W and Wong S 1998 The use of DIG-labelled cRNA probes for the detection of cymbidium mosaic potexvirus (CymMV) and odontoglossum ringspot tobamovirus (ORSV) in orchids *Journal of Virological Methods* **70** 193-9

[12] Buttry D and Ward M 1992 Measurement of interfacial processes at electrode surfaces with the electrochemical quartz crystal microbalance *Chemical Reviews* **92** 1355-79

[13] Huang G S, Wang M T and Hong M Y 2006 A versatile QCM matrix system for online and high-throughput bio-sensing *Analyst* **131** 382-7

[14] Rickert J, Brecht A and Gopel W 1997 QCM operation in liquids: constant sensitivity during formation of extended protein multilayers by affinity *Anal. Chem* **69** 1441-8

[15] Liu Y, Yu X, Zhao R, Shangguan D H, Bo Z Y and Liu G Q 2003 Quartz crystal biosensor for real-time monitoring of molecular recognition between protein and small molecular medicinal agents *Biosensors and Bioelectronics* **19** 9-19

[16] Lazerges M, Perrot H, Zeghib N, Antoine E and Compere C 2006 In situ QCM DNA-biosensor probe modification *Sensors and Actuators B-Chemical* **120** 329-37

[17] Eun A, Huang L, Chew F, Fong-Yau Li S and Wong S 2002 Detection of two orchid viruses using quartz crystal microbalance-based DNA biosensors *Phytopathology* **92** 654-8

[18] Tedeschi L, Citti L and Domenici C 2005 An integrated approach for the design and synthesis of oligonucleotide probes and their interfacing to a QCM-based RNA biosensor *Biosensors and Bioelectronics* **20** 2376-85

[19] Huang G S, Wang M T, Su C W, Chen Y S and Hong M Y 2007 Picogram detection of metal ions by melanin-sensitized piezoelectric sensor *Biosensors and Bioelectronics* **23** 319-25

[20] Eun A, Huang L, Chew F, Li S and Wong S 2002 Detection of two orchid viruses using quartz crystal microbalance (QCM) immunosensors *Journal of Virological Methods* **99** 71-9

[21] Selvaraju T and Ramaraj R 2005 Electrochemically deposited nanostructured platinum on Nafion coated electrode for sensor applications *Journal of Electroanalytical*

Chemistry **585** 290-300

[22] McFarland A and Van Duyne R 2003 Single silver nanoparticles as real-time optical sensors with zeptomole sensitivity *Nano Letters* **3** 1057-62

[23] Serra A, Filippo E, Re M, Palmisano M, Vittori-Antisari M, Buccolieri A and Manno D 2009 Non-functionalized silver nanoparticles for a localized surface plasmon resonance-based glucose sensor *Nanotechnology* **20** -

[24] Patolsky F, Zheng G F, Hayden O, Lakadamyali M, Zhuang X W and Lieber C M 2004 Electrical detection of single viruses *Proceedings of the National Academy of Sciences of the United States of America* **101** 14017-22

[25] Someya T, Small J, Kim P, Nuckolls C and Yardley J 2003 Alcohol vapor sensors based on single-walled carbon nanotube field effect transistors *Nano Lett* **3** 877–81

[26] Erickson D, Mandal S, Yang A H J and Cordovez B 2008 Nanobiosensors: optofluidic, electrical and mechanical approaches to biomolecular detection at the nanoscale *Microfluidics and Nanofluidics* **4** 33-52

[27] Chen R, Bangsaruntip S, Drouvalakis K, Wong Shi Kam N, Shim M, Li Y, Kim W, Utz P and Dai H 2003 Noncovalent functionalization of carbon nanotubes for highly specific electronic biosensors *Proceedings of the National Academy of Sciences* **100** 4984-9

[28] Wong S M, Mahtani P H, Lee K C, Yu H H, Tan Y, Neo K K, Chan Y, Wu M and

Chng C G 1997 Cymbidium mosaic potexvirus RNA: complete nucleotide sequence and phylogenetic analysis *Archives of Virology* **142** 383-91

[29] Shim M, Kam N, Chen R, Li Y and Dai H 2002 Functionalization of carbon nanotubes for biocompatibility and biomolecular recognition *Nano Letters* **2** 285-8

[30] Chen R, Zhang Y, Wang D and Dai H 2001 Noncovalent sidewall functionalization of single-walled carbon nanotubes for protein immobilization *J. Am. Chem. Soc* **123** 3838-9

[31] Hartschuh A, S nchez E, Xie X and Novotny L 2003 High-resolution near-field Raman microscopy of single-walled carbon nanotubes *Physical Review Letters* **90** 95503

Contents Ⅱ

Chapter 1: Introduction

Cymbidium mosaic virus (CymMV) was reported for the first time by Jensen [1, 2]. CymMV has been recognized to be an infectious disease to many orchids [3, 4]. The virus was induced the mosaic or black streak in cymbidium orchids and it's the most prevalent and economically important viruses [5].

In recent research, many methods have been developed for analyzing CymMV, for example, enzyme-linked immunosorbent assay (ELISA) [6], reverse transcription polymerase chain reaction (RT–PCR) [7], immuno-capillary zone electrophoresis (I-CZE) [8], Liquid chromatography:mass spectrometry (LC/MS) and matrix-assisted laser desorption-ionization (MALDI) [9], DIG-labelled cRNA probes [10]. Some of them require additional timely labeling and amplification procedures. These methods are sensitive however it takes hours and trained personnel to obtain unambiguous results.

QCM is a mass-detection device that operates based on the piezoelectric properties of quartz crystal [11-13]. Because of their extraordinary sensitivity and stability, QCM have been applied in recent years as biosensors for the online detection of biomolecules such as protein, DNA, RNA and metal ion [14-18]. QCM is also applied in the detection of CymMV and elicits the advantages of convenience and economy. However, sensitivity and stability might be improved by further modification [19].

Gold nanoparticles (GNPs) have been used to modify sensors, such as electronic sensor [20, 21], glucose sensor [22], optical sensor [23], surface plasmon resonance sensor [24], and capillary electrophoresis [25] could significantly improve the sensitivity. Surface modification of QCM electrode using gold nanoparticle-modified nanowire [26] and single strain DNA probe linked to the gold nanoparticle surface [27] are performed; however, the enhancement of sensitivity and capacity are yet to be demonstrated.

The current study is based on the hypothesis that gold nanoparticles modification of the QCM electrode is capable of enhancing the sensitivity and capacity for the detection of CymMV. Increase in surface charge and surface energy was discussed. Compared to the traditional detection methods, our study provides a convenient, economic, and time-saving method with comparable sensitivity to detection of CymMV.

Chapter 2: Experiment detail

2.1 QCM experiment

An oscillator (Catalog #35366-10) and a flow cell (Catalog#35363) were purchased from International Crystal Manufacturing Co. (Oklahoma City, USA). The QCM was fabricated from a 0.2-mm thick AT-cut quartz wafer. A laboratory-constructed transistor–transistor logic integrated circuit (TTLIC) was used to power the QCM. An Agilent HP 53132 universal frequency counter was used to monitor the frequency output.

2.2. CymMV purification and antisera production

CymMV was purified according to Wong and coworkers [28]. Fresh CymMV-infected leaves (100 g) were homogenized in a Waring blender (Waring Products, New Hartford, CT) for 5 min with 500 mL of extraction buffer (0.1% beta-mercaptoethanol, 0.01 M EDTA, and 0.1 M sodium phosphate buffer, pH 7.5). The extract was clarified with 100 mL of chloroform and centrifuged at 8,000 g for 10 min at 4°C. The supernatant was filtered through cheesecloth before sodium chloride (NaCl) and polyethylene glycol (molecular weight 8,000) were added to concentrations of 0.25 and 4%, respectively. The mixture was centrifuged at 8,000 g for 20 min at 4°C. The pellet was suspended in 5 mL of suspension buffer (1% Triton X-100 and 0.1 M sodium borate buffer, pH 8.0) and stirred slowly for 12 h at 4°C. The suspension was centrifuged at low speed (8,000 g) to remove debris, and the supernatant was

centrifuged at 90,000 g for 2.5 h at 4°C. The pellet was suspended in 2 mL of 0.01 M sodium borate buffer, pH 7.5, and stored at –20°C. The purified CymMV were characterized by SEM (figure 1). The CymMV particle lengths ranged from about 40 nm to 550 nm, with a width of approximately 15 nm. The scale bar is 100 nm.

Purified CymMV virus (1 mg) were suspended in 1 mL of 0.02 M sodium phosphate buffer, pH 7.0, and emulsified with an equal volume of Freund's incomplete adjuvant (Sigma-Aldrich Corp., St. Louis) by vortexing for 1 min. The resulting emulsion was injected intramuscularly into the hind legs of a New Zealand White rabbit. Boost injections of 1 mg each were administered 14, 21, and 28 days after the first injection. Before each boost injection was administered, 10 mL of blood was drawn from the ear of the rabbit. The antiserum collected was divided into 1 mL aliquots and stored at 4°C.

2.3. Preparation and characterization of gold nanoparticles

Seed colloids were prepared by adding 1 ml of 0.25 mM $HAuCl_4$ to 90 ml of H_2O and stirring for 1 min at 25 ◦C [29, 30]. Then 2 ml of 38.8 mM sodium citrate were added to the solution, which was stirred for 1 min, followed by the addition of 0.6 ml freshly prepared 0.1 M $NaBH_4$ in 38.8 mM sodium citrate. 37 nm gold nanoparticles were generated by adjusting the volume of sodium citrate, seed colloid, and reaction temperature. The solution was stirred for an additional 5–10 min at 0–4 ˚C. The reaction temperature and reaction time were adjusted to obtain GNPs of larger size. The 37 nm GNPs were characterized by UV

absorbance and examined with electron microscopy (EM) for size and homogeneity.

2.4. Fabrication of GNP-modified QCM

The gold electrode was cleaned by immersing in 1.2 M NaOH for 20 min, 1.2 M HCl for 5 min, and distilled water for 5 min; after a final rinse with 95% alcohol, it was air-dried at room temperature.

Then the QCM was modified with various concentration of 1,6-hexanedithiol in ethanol for 30 min. Immobilization of 37 nm GNPs onto the thiol-modified surfaces was performed in aqueous GNPs for 1 h at room temperature and washed briefly with distilled water. Then, the plate surface was treated with 4 mg ml^{-1} 3,3′-Dithiodipropionic acid di(N-hydroxysuccinimide ester (DTSP) (Sigma-Aldrich Corp) solution in DMSO (Fluka) (the DTSP solution was reduced by same amount of dithiothreitol, DTT) for 2 h and washed with deionized water. The samples were then incubated in 1 μg mL^{-1} anti-CymMV IgG in PBS for 4 h and washed with PBS buffer for 1 min, then with deionized water. Blocking was achieved by adding 1mg ml^{-1} BSA, incubating overnight before detection. Naked electrode modification was absent GNPs crosslinked step as control experiment. The sample was examined with scanning electron microscopy (SEM) for size and homogeneity. Surface charges were measured by SCA-2500 Surface Charge Analyzer. Additionally, the frequencies of all QCMs were monitored until steady state conditions were achieved (usually 30 min to 1 h; then, 20 μL sample was injected).

Chapter 3: Results and discussion

3.1. Surface modification of GNP enhanced sensitivity for QCM detection of CymMV

To evaluate enhancing ability of nanoparticle modification to QCM, gold electrode was functionalized by 37 nm GNP through 1,6-hexanedithiol as cross-linker. The modified electrode was reacted with DTSP. Antibodies were conjugated to N-Hydroxysuccinimide (NHS) group of DTSP for virus detection (Figure 1).

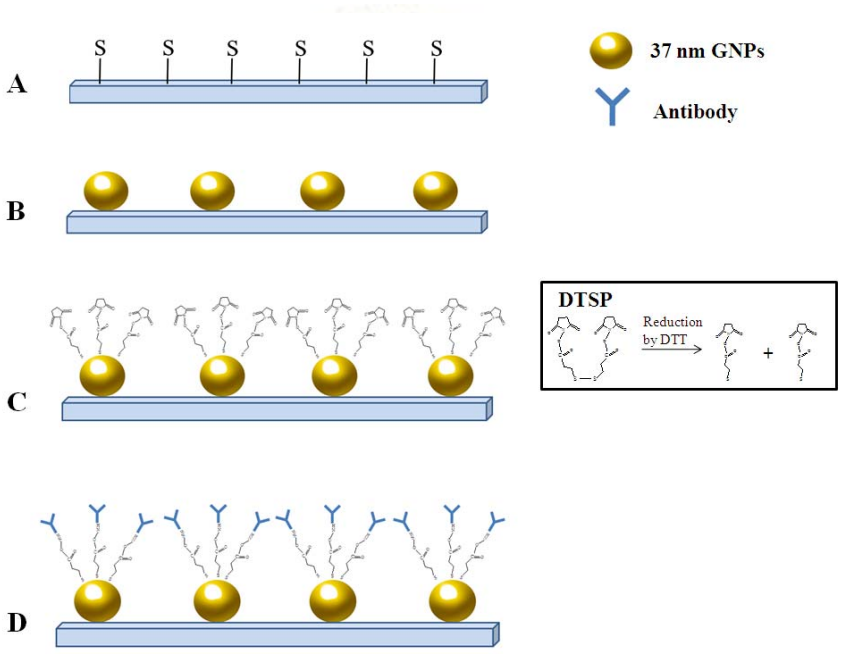

Figure 1. Schematic representation for the step-by step modification of QCM electrode using 37 nm GNP. GNPs were cross-linked to the gold electrode by 1,6-hexanedithiol, followed by reaction with DTSP. Antibodies were conjugated to NHS group of DTSP for virus detection

The purified CymMV were quantified by UV absorbance at 280 nm and visualized by

SEM (Figure 2).

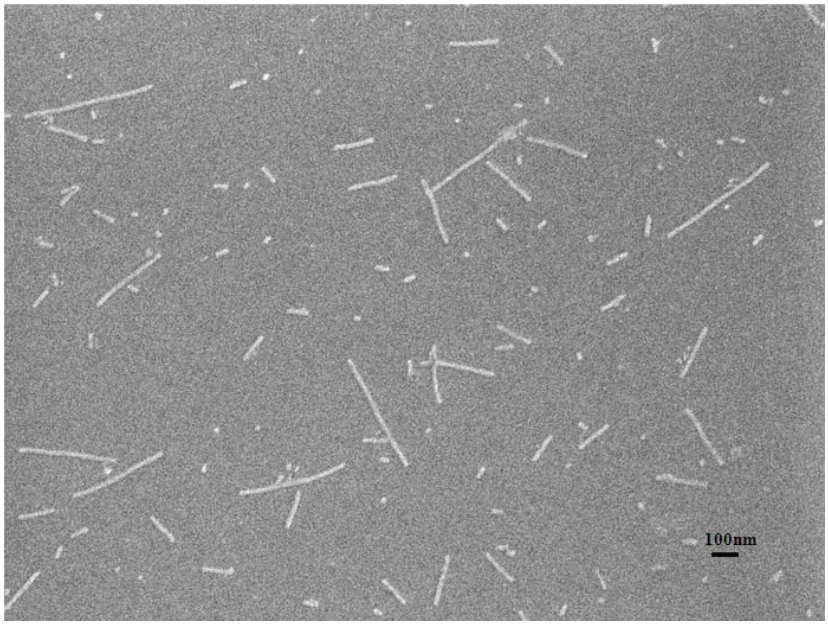

Figure 2. SEM image of purified CymMV. The particle lengths ranged from about 40 nm to 550 nm, with widths of approximately 15 nm. The scale bar is 100 nm.

Twenty microliters of properly diluted CymMV were injected into the QCM-FIA system and monitored by resonanting frequency in real time (Figure 3).

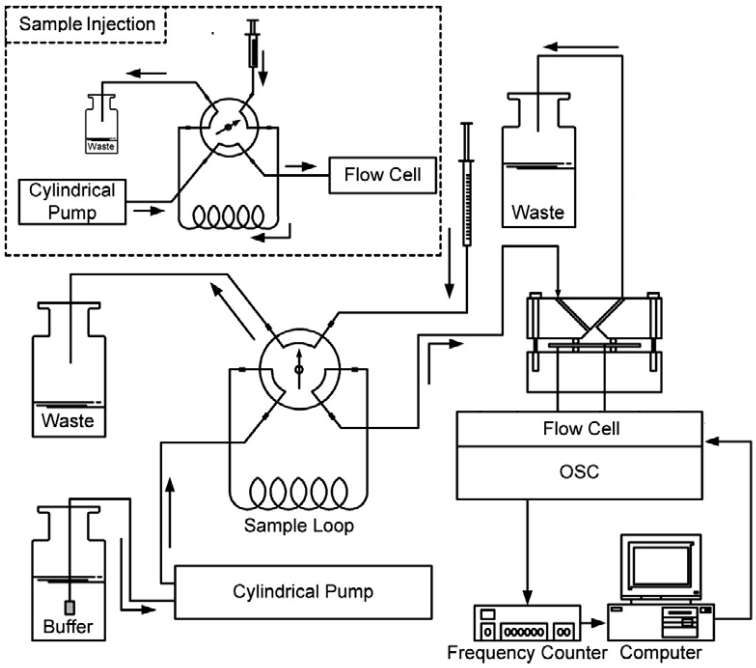

Figure 3. Schematic representation for the QCM flow injection analysis apparatus. Continuous flow was achieved using a cylindrical pump. The sample was injected through an injection loop and pumped into flow cell.

Modification of 37 nm GNPs with 0.5 v/v % of 1,6-hexanedithiol enhanced the frequency shift of QCM. The naked electrode responded to 208 ng CymMV by 122.2 Hz, while the functionalized QCM respond to 208 ng CymMV by 591 Hz (Figure 4). A 10-fold enhancement of sensitivity was observed at 0.52 ng CymMV, from 4.62 Hz ng^{-1} to 48.1 Hz ng^{-1} (Table 1). Limit of detection (LOD) is defined as three times standard deviation of background noise (S/N>3, noise ≒ 0.48 Hz). The LOD of naked QCM was 1 ng ($5x10^{-2}$ μg

mL^{-1}); while the LOD of was and 0.1 ng ($5x10^{-3}$ µg mL^{-1}) for 37 nm GNP-modified QCM (Figure 5). Modification of GNP on the electrode enhanced 10 folds in sensitivity and in LOD.

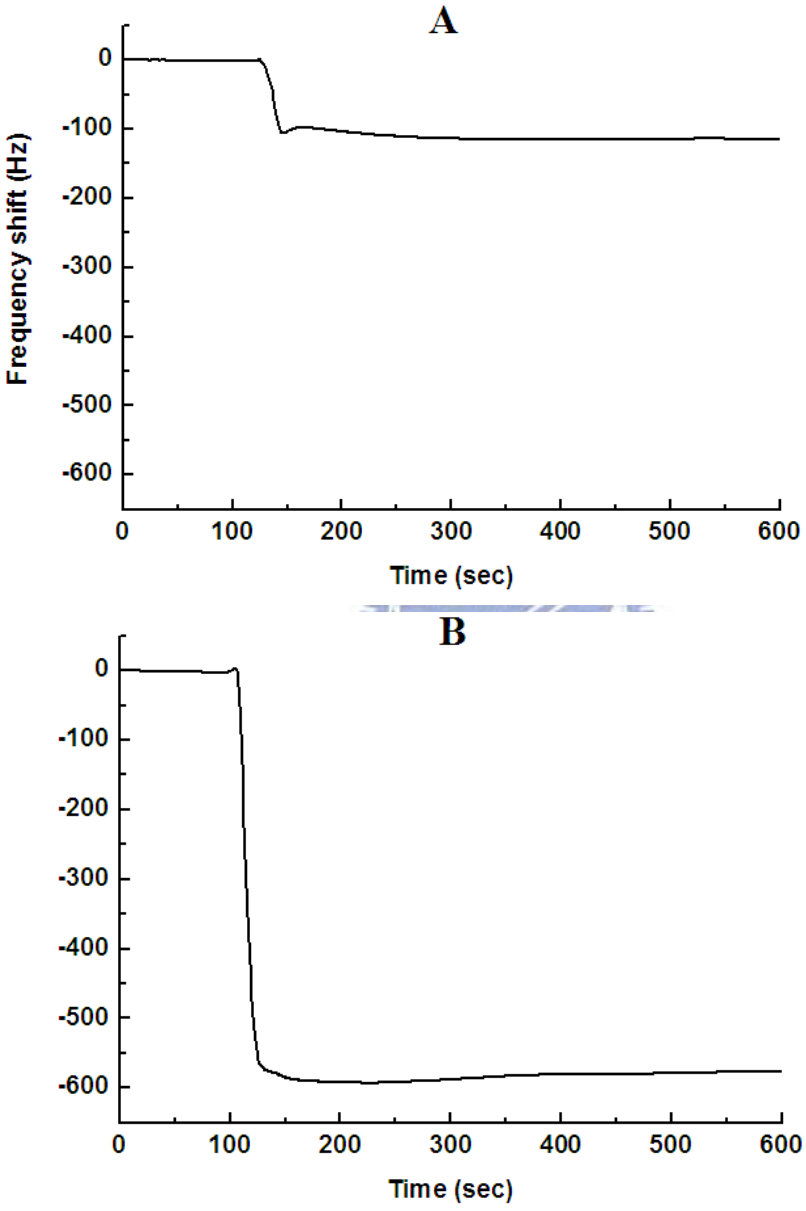

Figure 4. Frequency response for the detection of CymMV. The frequency shift was monitored by injection of 20 µl of CymMV (10 µg ml^{-1}). (A) Unmodified QCM and (B) GNP-modified QCM.

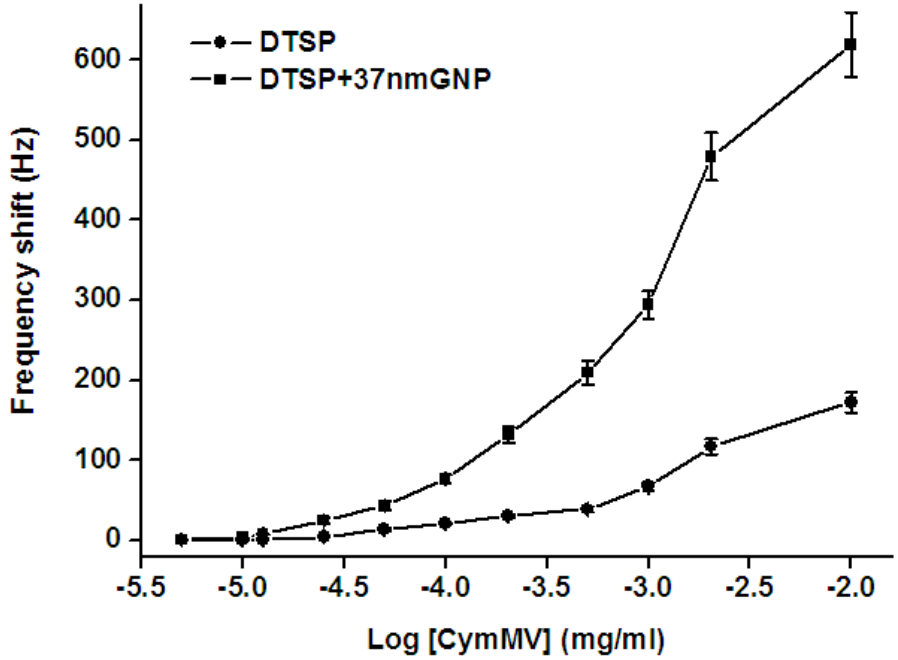

Figure 5. Comparison for the frequency shift versus applied CymMV for naked and GNP-modified QCM. Various concentrations of purified CymMV are injected into the QCM-FIA system equipped with naked QCM sensor and GNP-modified QCM sensor. Each value is averaged from 6 independent injections.

Table. 1 Comparison of the sensitivities of naked QCMs and GNP-modified QCMs

CymMV (μg mL^{-1})	Sensitivity [a] (Hz ng^{-1})	
	Naked	37 nm GNP
10.34	0.83	2.99
2.068	2.77	11.3
1.034	3.24	14.2
0.517	3.76	20.2
0.258	7.23	31.3
0.103	7.99	37.2
0.052	5.66	41.8
0.026	4.62	48.1
0.013	3.11	30.3
0.010	3.44	19.5
0.005	4.56	26.6

[a] Sensitivity is defined as changes in frequency shift per applied virus weight. Injection volume is 20 μL. Sensitivity(S) = $\Delta F/\Delta m$. ΔF: Frequency shift; Δm: apply weight.

3.2. Correlation between surface charge of gold electrode and sensitivity

QCM is a mass-detection device that operates based on the piezoelectric properties of quartz crystal. The piezoelectric effect is proportional to fundamental resonating frequency (F_0). QCM frequency shift might be enhanced through the elevation of fundamental resonating frequency. Modification of GNP on the electrode increased surface plasmon resonance (SPR) which intensified surface charges and electric field on gold electrode. Consequently, the fundamental resonating frequency was shifted.

By changing the concentration of 1,6-hexanedithiol from 0.1 % to 1 %, various coverage of 37 nm GNPs onto QCM electrode were achieved which ranged from 8.3% to 35.5% (Figure 6).

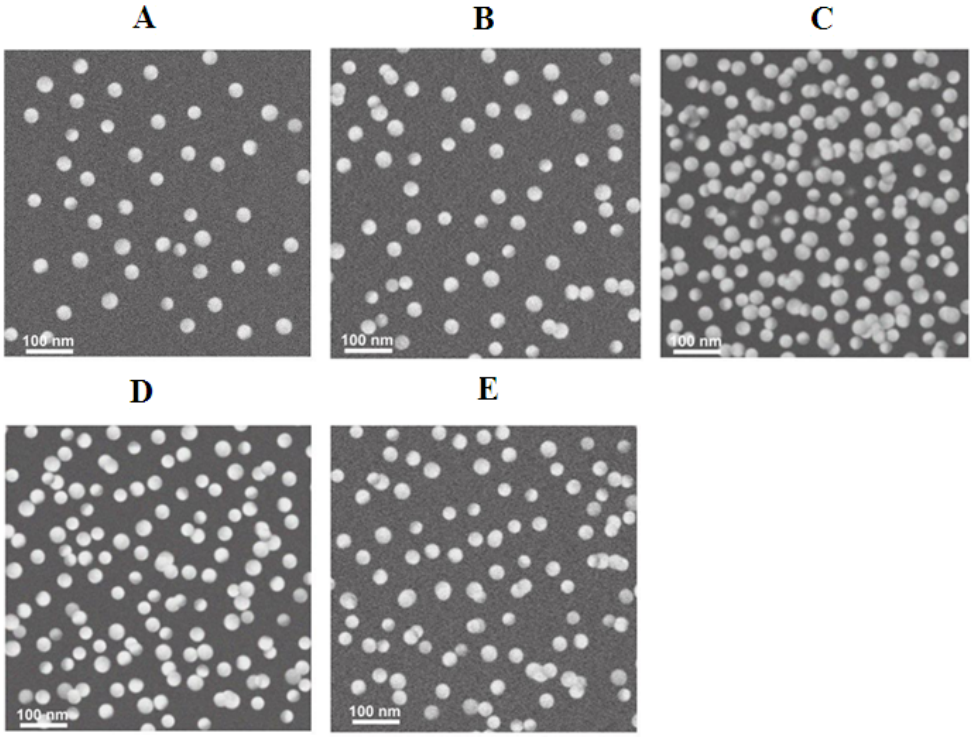

Figure 6. SEM images of electrodes with various concentrations of 1,6-hexanedithio applied during surface modification using 37nm GNPs. (A) 0.1 v/v% (B) 0.3 v/v% (C) 0.5 v/v% (D) 0.7 v/v% (E) 1 v/v %.

SEM image showed that the maximum coating density occurred at 0.5 v/v % of 1,6-hexanedithiol which covered 35.5 % of the surface. Surface charges of 37 nm GNPs functionalize electrode were measured (Table 2).

Table. 2 Surface charges and fundamental resonating frequency at various concentrations of 1,6-hexanedithiol

1,6-hexanedithiol (v/v %)	Coverage (%)	Surface charges (nC)	ΔF_0 (Hz)
0.1	8.32	2091.90	2146.5
0.3	12.1	3525.45	9591.2
0.5	35.7	12893.1	23281.0
0.7	24.4	6659.92	18019.0
1	17.3	5144.59	13932.0

ΔF_0: Fundamental resonating frequency shift of 10MHz QCM. Naked QCM was monitored as F_1. Various concentrations of 1,6-hexanedithiol modification of 37nm GNPs were monitored as F_2. $\Delta F_0 = (F_1 - F_2)$.

Linear correlation of total surface charge to fundamental resonating frequency was elicited with correlation coefficient of 0.991 (Figure 7). According to the Sauerbrey equation (1):

$$\Delta F = -2F_0^{\,2} x\, 2\Delta m / A(\mu_q \rho_q)^{1/2} \quad (1)$$

Where ΔF, Δm are the frequency and mass change, A is the piezoelectric active area, μ_q is the shear modulus, ρ_q is the density of quartz. The sensitivity ($S = \Delta F/\Delta m$) was enhanced with total surface charges increase.

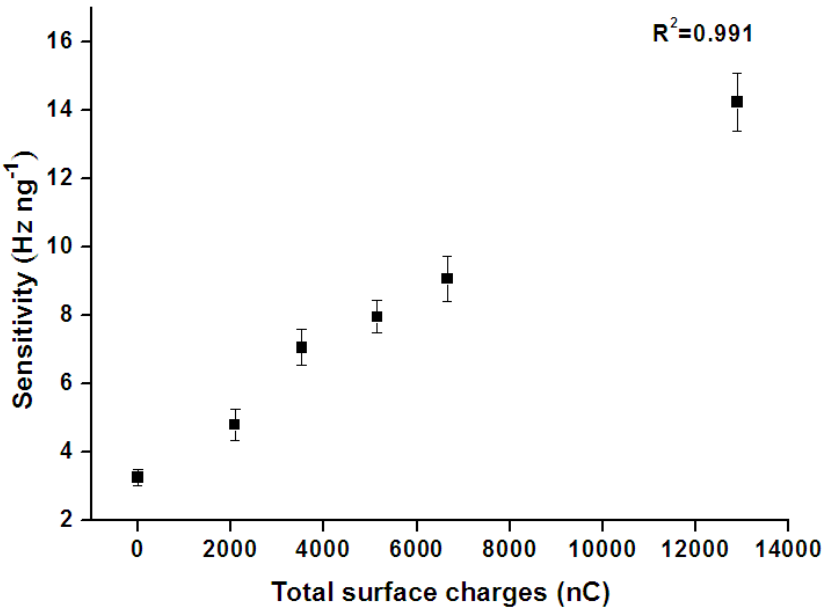

Figure 7. Correlation between sensitivity and surface charge of electrodes.

3.3. Correlation between surface energy of gold electrode and detecting capacity

GNP modification increased surface area and possibly increased the surface energy of QCM electrode. Total surface energy is a parameter that affects self-assemble (SAM). Surface energy (γ) of a phase can be expressed as $\gamma = \gamma^{LW} + \gamma^{AB} = \gamma^{LW} + 2\,(\gamma_L^{+}\,\gamma_L^{-})^{1/2}$, where γ^{LW} and γ^{AB} represent the dispersion (apolar) and polar terms of the surface tension, respectively, and γ^{+} and γ^{-} are the electron acceptor and electron donor parameters, respectively, in the polar part. The contact angle equilibrium, based on the Young–Dupre equation [31], was formulated to describe the interfacial tension between the liquid (L) and the surface (S) (2) [32]:

$$(1 + \cos\theta)\,\gamma_L = 2(\gamma_L^{LW}\,\gamma_L^{LW})^{1/2} + (\gamma_S^{+}\,\gamma_L^{-})^{1/2}(\gamma_L^{+}\,\gamma_S^{-})^{1/2} \qquad (2)$$

Where θ is the contact angle determined using three liquids include water, ethylene, and diiodomethane with known values of γ_L^{LW}, γ_L^+, and γ_L^-. Contact angles of electrode at each step during surface modification were measured. Corresponding total surface energy was calculated based on the above equation (Figure 8). GNPs modification at 0.5% 1,6-hexanedithiol increased total surface energy from 51.22 mJ cm^{-2} to 63.07 mJ cm^{-2}.

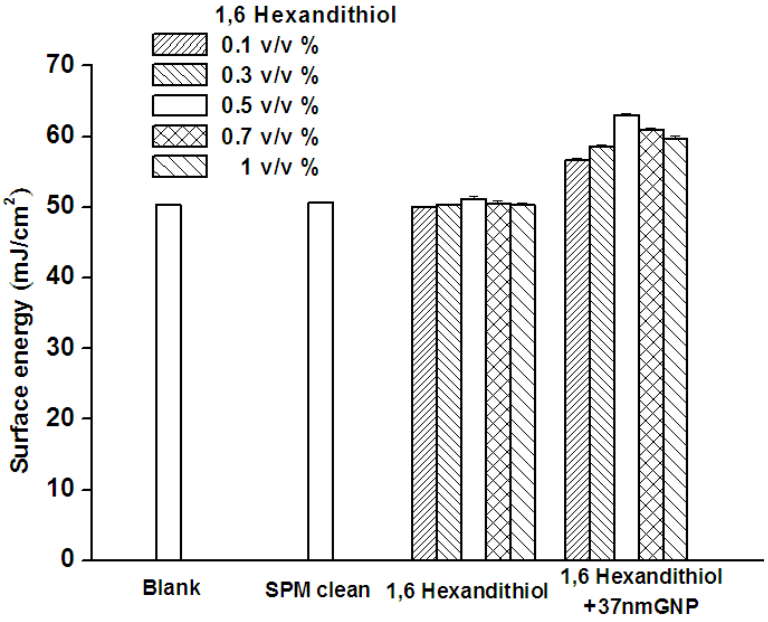

Figure 8. Calculated total surface energy of electrodes after each step of GNP modification. Contact angles are measured for blank electrodes, after cleaning by SPM, after 1,6-hexanedithiol treatment, and after GNP coating. Total surface energies are calculated. Maximum total surface energy occurs to 0.5% GNP modification with 35% coverage of the surface.

The binding capacity might be enlarged due to the increase in surface area and total surface energy. Binding capacity might be monitored by the increase in available DTSP

which can be quantified by FTIR. Intensity of the characteristic absorbance at 1740 cm^{-1} 1778 cm^{-1} for C=O bond, 1078 cm^{-1} for C-N bond, and 1207 cm^{-1} for C-N-O bond was measured (Figure 9).

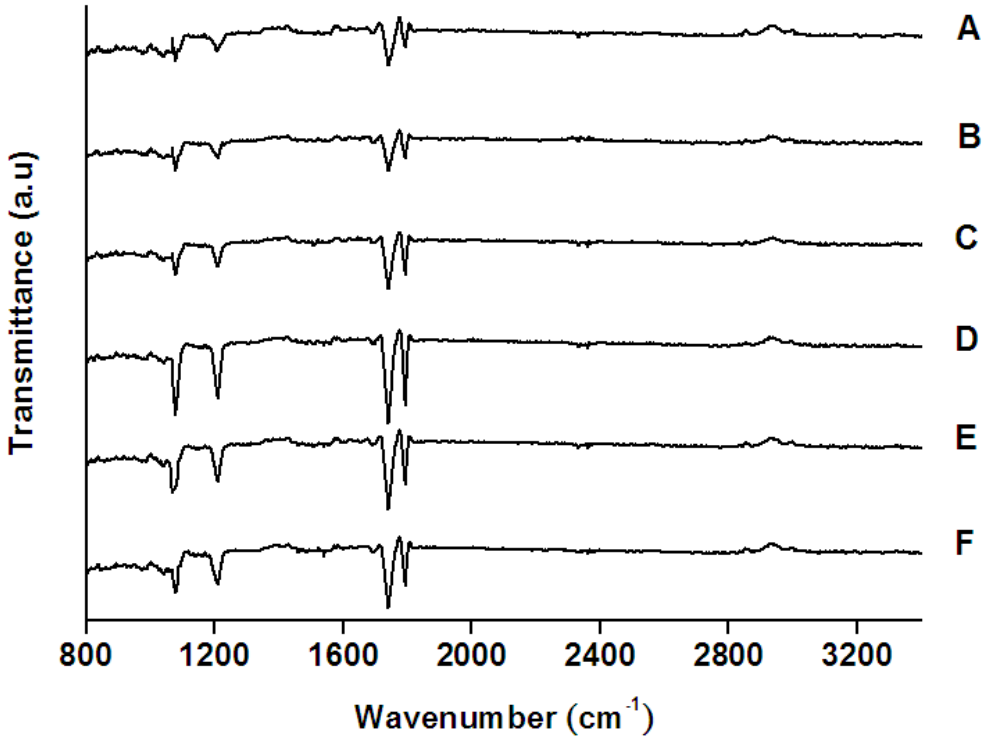

Figure 9. IR spectra of QCM electrode after modification of DTSP. DTSP were crosslinked to the GNP-coated electrodes modified by various concentrations of 1,6-hexanedithiol. FTIR are taken for (A) Naked QCM (B) 0.1 v/v% (C) 0.3 v/v% (D) 0.5 v/v% (E) 0.7 v/v%, and (F) 1 v/v %.

Positive correlation was elicited between the averaged intensity of characteristic functional groups (C=O, C-N, and C-N-O bonds) and total surface energy with correlation coefficient of 0.883 (Figure 10). In summary, GNPs modification elevated the surface energy which is correlated to the binding capacity of QCM.

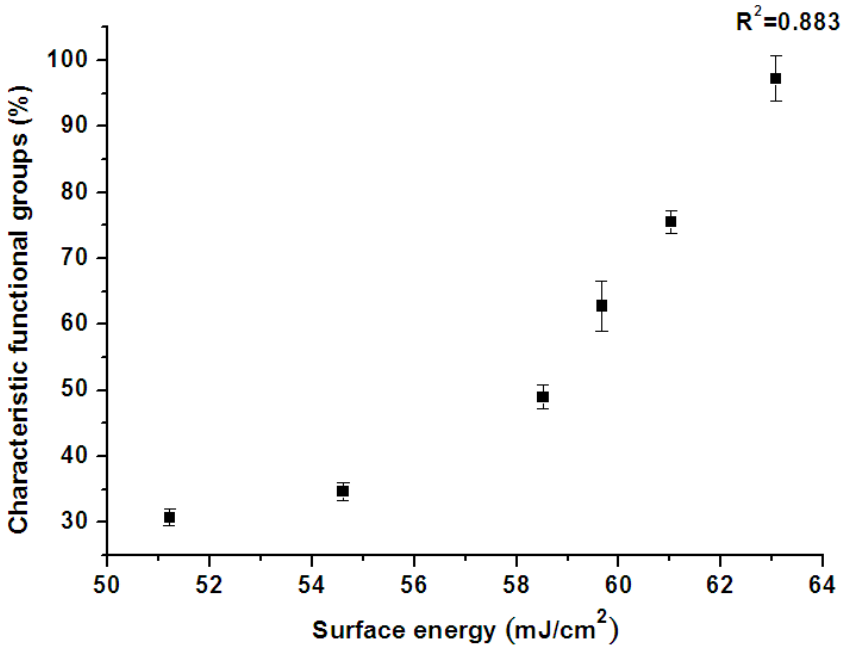

Figure 10. Correlation between concentration of DTSP and total surface energy. Relative concentrations of DTSP are measured by the averaged intensities for the characteristic frequencies at 1740 cm^{-1} 1778 cm^{-1} for C=O bond, 1078 cm^{-1} for C-N bond, and 1207 cm^{-1} for C-N-O bond in FTIR spectra. The relative concentrations are calculated using concentration of DTSP at 35% GNP coverage as control.

4. Conclusion

We modified the surface of QCM electrode with 37-nm GNP and found that the sensitivity and capacity of detection was enhanced. Maximum surface coverage of 35% occurred when 0.5% 1,6-hexanedithiol was applied. A 10-fold enhancement of sensitivity was observed at 0.52 ng CymMV, from 4.62 Hz ng^{-1} to 48.1 Hz ng^{-1}. Limit of detection is improved from 1 ng to 0.1 ng. Modification of GNP enhanced 10 folds in sensitivity and in LOD. Increase in surface charge was observed which correlates with the sensitivity of modified QCM. Increase in surface energy was observed which was correlated to the increased in binding capacity of QCM electrode.

References

[1] Jensen D 1950 Mosaic of Cymbidium orchids *Phytopathology* **40** 966-7

[2] Jensen D 1951 Mosaic or black streak disease of Cymbidium orchids *Phytopathology* **41** 401-14

[3] Hu J, Ferreira S, Wang M and Xu M 1993 Detection of cymbidium mosaic virus, odontoglossum ringspot virus, tomato spotted wilt virus, and potyviruses infecting orchids in Hawaii *Plant Dis* **77** 464-8

[4] Zettler F W, Ko N J, Wisler G C, Elliott M S and Wong S M 1990 Viruses of Orchids and Their Control *Plant Disease* **74** 621-6

[5] Pearson M N and Cole J S 1991 Further Observations on the Effects of Cymbidium Mosaic-Virus and Odontoglossum Ringspot Virus on the Growth of Cymbidium Orchids *Journal of Phytopathology-Phytopathologische Zeitschrift* **131** 193-8

[6] Vejaratpimol R, Channuntapipat C, Liewsaree P, Pewnim T, Ito K, Iizuka M and Minamiura N 1998 Evaluation of enzyme-linked immunosorbent assays for the detection of Cymbidium mosaic virus in orchids *Journal of Fermentation and Bioengineering* **86** 65-71

[7] Eun A J C, Seoh M L and Wong S M 2000 Simultaneous quantitation of two orchid viruses by the TaqMan (R) real-time RT-PCR *Journal of Virological Methods* **87** 151-60

[8] Eun A and Wong S 1999 Detection of Cymbidium mosaic potexvirus and Odontoglossum ringspot tobamovirus using immuno-capillary zone electrophoresis *Phytopathology* **89** 522-8

[9] Tan S W, Wong S M and Kini R M 2000 Rapid simultaneous detection of two orchid viruses using LC- and/or MALDI-mass spectrometry *J Virol Methods* **85** 93-9

[10] Hu W and Wong S 1998 The use of DIG-labelled cRNA probes for the detection of cymbidium mosaic potexvirus (CymMV) and odontoglossum ringspot tobamovirus (ORSV) in orchids *Journal of Virological Methods* **70** 193-9

[11] Buttry D and Ward M 1992 Measurement of interfacial processes at electrode surfaces with the electrochemical quartz crystal microbalance *Chemical Reviews* **92** 1355-79

[12] Huang G S, Wang M T and Hong M Y 2006 A versatile QCM matrix system for online and high-throughput bio-sensing *Analyst* **131** 382-7

[13] Rickert J, Brecht A and Gopel W 1997 QCM operation in liquids: constant sensitivity during formation of extended protein multilayers by affinity *Anal. Chem* **69** 1441-8

[14] Liu Y, Yu X, Zhao R, Shangguan D H, Bo Z Y and Liu G Q 2003 Quartz crystal biosensor for real-time monitoring of molecular recognition between protein and small molecular medicinal agents *Biosensors & Bioelectronics* **19** 9-19

[15] Lazerges M, Perrot H, Zeghib N, Antoine E and Compere C 2006 In situ QCM DNA-biosensor probe modification *Sensors and Actuators B-Chemical* **120** 329-37

[16] Eun A, Huang L, Chew F, Fong-Yau Li S and Wong S 2002 Detection of two orchid viruses using quartz crystal microbalance-based DNA biosensors *Phytopathology* **92** 654-8

[17] Tedeschi L, Citti L and Domenici C 2005 An integrated approach for the design and synthesis of oligonucleotide probes and their interfacing to a QCM-based RNA biosensor *Biosensors and Bioelectronics* **20** 2376-85

[18] Huang G S, Wang M T, Su C W, Chen Y S and Hong M Y 2007 Picogram detection of metal ions by melanin-sensitized piezoelectric sensor *Biosensors & Bioelectronics* **23** 319-25

[19] Eun A, Huang L, Chew F, Li S and Wong S 2002 Detection of two orchid viruses using quartz crystal microbalance (QCM) immunosensors *Journal of Virological Methods* **99** 71-9

[20] Xiao Y, Patolsky F, Katz E, Hainfeld J and Willner I 2003 Plugging into Enzymes": Nanowiring of Redox Enzymes by a Gold Nanoparticle. pp 1877-81

[21] Park S, Taton T and Mirkin C 2002 Array-based electrical detection of DNA with nanoparticle probes. pp 1503-6

[22] Bharathi S and Nogami M 2001 A glucose biosensor based on electrodeposited biocomposites of gold nanoparticles and glucose oxidase enzyme *The Analyst* **126** 1919-22

[23] Himmelhaus M and Takei H 2000 Cap-shaped gold nanoparticles for an optical biosensor *Sensors & Actuators: B. Chemical* **63** 24-30

[24] Hu W, Chen S, Huang K, Hsu J, Chen W, Chang G and Lai K 2004 A novel ultrahigh-resolution surface plasmon resonance biosensor with an Au nanocluster-embedded dielectric film *Biosensors and Bioelectronics* **19** 1465-71

[25] Huang M, Kuo Y, Huang C and Chang H 2004 Separation of long double-stranded DNA by nanoparticle-filled capillary electrophoresis *Anal. Chem* **76** 192-6

[26] Tang D, Yuan R and Chai Y 2008 Quartz crystal microbalance immunoassay for carcinoma antigen 125 based on gold nanowire-functionalized biomimetic interface *The Analyst* **133** 933-8

[27] Liu T, Tang J and Jiang L 2004 The enhancement effect of gold nanoparticles as a surface modifier on DNA sensor sensitivity *Biochemical and Biophysical Research Communications* **313** 3-7

[28] Wong S M, Mahtani P H, Lee K C, Yu H H, Tan Y, Neo K K, Chan Y, Wu M and Chng C G 1997 Cymbidium mosaic potexvirus RNA: complete nucleotide sequence and phylogenetic analysis *Archives of Virology* **142** 383-91

[29] Brown K, Walter D and Natan M 2000 Seeding of colloidal Au nanoparticle solutions. 2. Improved control of particle size and shape *Chemistry of Materials* **12** 306-13

[30] Chithrani B, Ghazani A and Chan W 2006 Determining the size and shape dependence

of gold nanoparticle uptake into mammalian cells *Nano Lett* **6** 662-8

[31] Van Oss C, Chaudhury M and Good R 1988 Interfacial Lifshitz-van der Waals and polar interactions in macroscopic systems *Chem. Rev* **88** 927-41

[32] Ko F, Wu C, Chen M, Chen J and Chu T 2007 Soft-mold-induced self-construction of polymer patterns under microwave irradiation *Applied Physics Letters* **90** 191901